

# SMURF-seq: efficient short-read sequencing on long-read sequencers

Rishvanth K. Prabakar

Quantitative and Computational Biology Section,  
Department of Biological Sciences,  
University of Southern California,  
1050 Childs Way,  
Los Angeles 90089, USA

July 15, 2020

# Contents

<b>1</b>	<b>Introduction</b>	<b>3</b>
<b>2</b>	<b>Background</b>	<b>4</b>
2.1	Nanopore sequencing . . . . .	4
2.2	Copy number variation and profiling . . . . .	4
2.3	Prior protocols based on concatenating DNA molecules . . . . .	4
<b>3</b>	<b>Sampling molecules using re-ligated fragments (SMURF)-seq</b>	<b>5</b>
3.1	Motivation . . . . .	5
3.2	SMURF-seq protocol . . . . .	6
3.3	Mapping SMURF-seq reads . . . . .	9
3.3.1	Simulating SMURF-seq reads to evaluate mapping programs . . . . .	9
3.3.2	Evaluating performance using simulated SMURF-seq reads . . . . .	9
3.3.3	Data sets for generating simulated SMURF-seq reads . . . . .	10
3.3.4	Initial selection of mapping tools . . . . .	10
3.3.5	Detailed evaluation and parameter optimization . . . . .	11
3.4	Efficient CNV profiling using SMURF-seq . . . . .	12
3.4.1	Normalizing restriction site bias . . . . .	12
3.4.2	Accurate CNV profiles using SMURF-seq . . . . .	12
3.4.3	Concordant profiles from fewer countable fragments . . . . .	13

# List of Figures

3.1	SMURF-seq efficiently sequences short fragments of DNA for read-counting applications with a reference genome on long-read sequencers, and yields up to 30 countable fragments per sequenced read. SMURF-seq sequences short DNA molecules by generating long concatenated molecules from these. SMURF-seq reads are aligned by splitting them into multiple fragments, each aligning to a distinct region in the genome. . . . .	6
3.2	Schematic of SMURF-seq protocol. SMURF-seq consists of four steps: restriction enzyme digestion, spin-column clean-up, re-ligation of fragmented DNA, and Ampure XP beads clean-up. . . . .	7
3.3	Restriction digestion and ligation of DNA molecules. (a) Distribution of length between restriction sites computed by measuring the distance between the recognition sites on the human reference genome. SaqAI recognizes the sequence TTAA and leaves a 2 bp overhang. (b) Negative gel image of fragmented and ligated normal diploid DNA using SaqAI restriction enzyme and T4 DNA ligase. Sticky-end and blunt-end ligation (by end-repair) of fragmented DNA are shown, and both yield ligated molecules of approximately the same length. . . . .	8
3.4	Accurate copy number profiles with SMURF-seq. (a) CNV profile of a normal diploid genome. Each blue point is a bin ratio to mean and the red line is the segmented bin ratio. (b) Superimposed CNV profiles of SK-BR-3 genome generated using SMURF-seq and Illumina WGS reads. (c) Venn diagram illustrating the accuracy of event calls using SMURF-seq compared with Illumina WGS. (d) Zoom-in of copy number changes on chromosome 8. (e) Scatter plot of bin ratio of SK-BR-3 genome using SMURF-seq and Illumina WGS reads. Pearson correlation of the data is shown. . . . .	13
3.5	Multiple SMURF-seq CNV profiles by multiplexing in a single run. (a) CNV profile of SK-BR-3 genome with down-sampled 10k SMURF-seq reads. (b) Scatter plot of normalized bin counts of the original SMURF-seq data and data down-sampled to 10k SMURF-seq reads. Pearson correlation of the data is shown. (c) CNV profile of barcode01 (Normal diploid genome) reads. (d) CNV profile of barcode02 (SK-BR-3 cancer genome) reads. (e) Scatter plot of bin ratios of SK-BR-3 genome using multiplexed SMURF-seq and Illumina WGS reads. . . . .	14

# **Chapter 1**

## **Introduction**

## **Chapter 2**

# **Background**

**2.1 Nanopore sequencing**

**2.2 Copy number variation and profiling**

**2.3 Prior protocols based on concatenating DNA molecules**

## Chapter 3

# Sampling molecules using re-ligated fragments (SMURF)-seq

### 3.1 Motivation

CNV profiling, and read-counting in general, can be done on nanopore sequencers with long reads following the standard sequencing procedure [2]. A typical Oxford MinION sequencing run generates approximately 500k reads (length  $\sim 8$  kb) [3, 4]. Read-counting applications in general do not benefit from longer reads beyond what is necessary for unique mapping to the reference genome. In these applications, for any fixed number of nucleotides sequenced, more information is obtained if those nucleotides are organized as more DNA molecules, rather than longer contiguous fragments.

In general, for a given sample of DNA, a nanopore instrument will generate more reads if the corresponding molecules are shorter. Once a molecule is loaded into a pore, the time spent sequencing is less for shorter reads. In addition, for a fixed amount of DNA, shorter molecules result in higher molar concentration when loaded onto the machine, increasing the rate at which each pore captures molecules [5, 6]. We verified this rationale by sequencing short DNA molecules (restriction enzyme digested normal diploid genome) using the Oxford MinION instrument. The sequencing run produced 2.58 million reads with a mean read length of 630.93 bp (data not shown). Using the same instrument, with SMURF-seq, we report here an average of 6.2 million mapped fragments per run, which is substantially more fragments than directly sequencing short reads.

The most important factor in the performance of SMURF-seq over sequencing short molecules directly is that sequencing concatenated fragments effectively eliminates the pore reload time for all but the first fragment in each read. However, there are a variety of additional factors that favor further optimization of the approach employed by SMURF-seq. First, reduction of resources spent on technical nucleotides: SMURF-seq uses a single barcode and sequencing adapter per read consisting of multiple fragments; sequencing short reads uses one barcode and adapter per fragment, adding approximately 50 bases to each fragment. This increases the time to sequence each short read. In sequencing short reads, as the reads get shorter the time consumed by these technical bases increases. In SMURF-seq, sequencing either shorter fragments in fixed length reads, or longer reads containing fragments of fixed average length, both reduce the time consumed sequencing these technical bases. In the limit, assuming 100bp DNA fragments, sequencing those fragments as short-reads corresponds to 33% technical nucleotides; for SMURF-seq, the portion of technical nucleotides remains low. Second, more nucleotides sequenced at full speed: We observed that the speed of sequencing was lower when sequencing short molecules. For example, the average sequencing speed was

315.54 bases per second for sequencing the diploid genome without SMURF-seq, and 400.29 bases per second when sequencing using SMURF-seq on the MinION sequencer. Third, leveraging optimizations to long-read protocols: The rapidly evolving nanopore library construction kits are continually optimized for long-read sequencing, and would likely require significant ad-hoc modifications to optimize sequencing of short molecules of length optimal for read-counting applications. SMURF-seq alleviates these drawbacks by using the nanopore instrument as intended for long-read sequencing, while generating the desired short fragments.

## 3.2 SMURF-seq protocol

The SMURF-seq protocol involves cleaving genomic DNA into short fragments, with length just sufficient for an acceptable rate of uniquely mapping fragments in the reference genome. These fragmented molecules are then randomly ligated back together to form artificial long DNA molecules, as required for long-read sequencing. The long re-ligated molecules are sequenced following the standard MinION library preparation protocol. After (or possibly concurrent with) sequencing, the SMURF-seq reads are mapped to the reference genome in a way that simultaneously splits them into their constituent fragments, each aligning to a distinct location in the genome (Fig. 3.1).

More specifically, genomic DNA is fragmented using restriction enzymes and ligated with T4 DNA ligase, with clean-up steps in between. SMURF-seq protocol is completely enzymatic and takes less than 90 minutes to complete (Fig. 3.2). The details of these steps are given below:

1. Restriction enzyme digestion: restriction enzymes recognize and cleave specific DNA sequences, typically producing sticky-ended DNA molecules. The choice of restriction enzyme used is primarily dependent on the size of the fragmented molecules produced. Based on the downstream application, they could also be influenced by other factors such as any bias they could introduce. An advantage of using

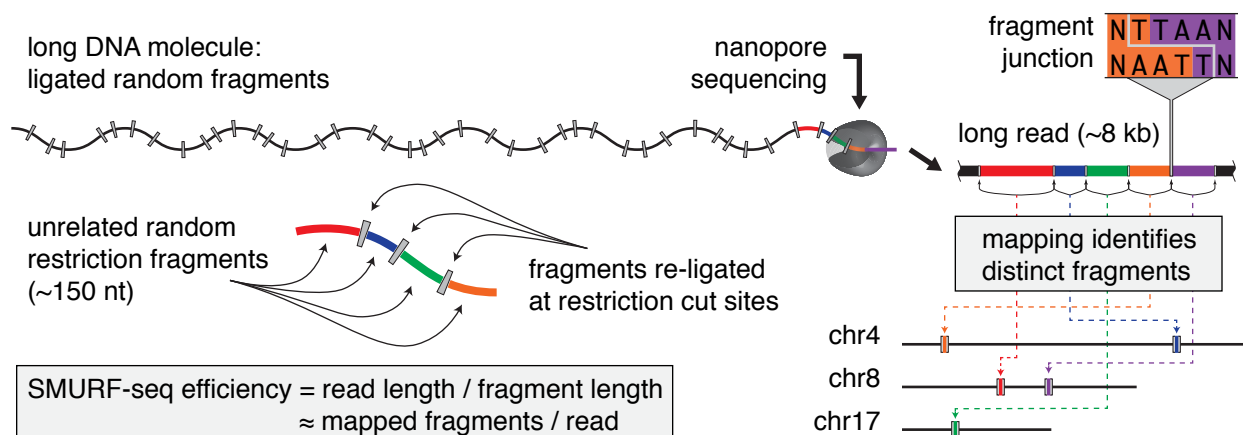


Figure 3.1: SMURF-seq efficiently sequences short fragments of DNA for read-counting applications with a reference genome on long-read sequencers, and yields up to 30 countable fragments per sequenced read. SMURF-seq sequences short DNA molecules by generating long concatenated molecules from these. SMURF-seq reads are aligned by splitting them into multiple fragments, each aligning to a distinct region in the genome.

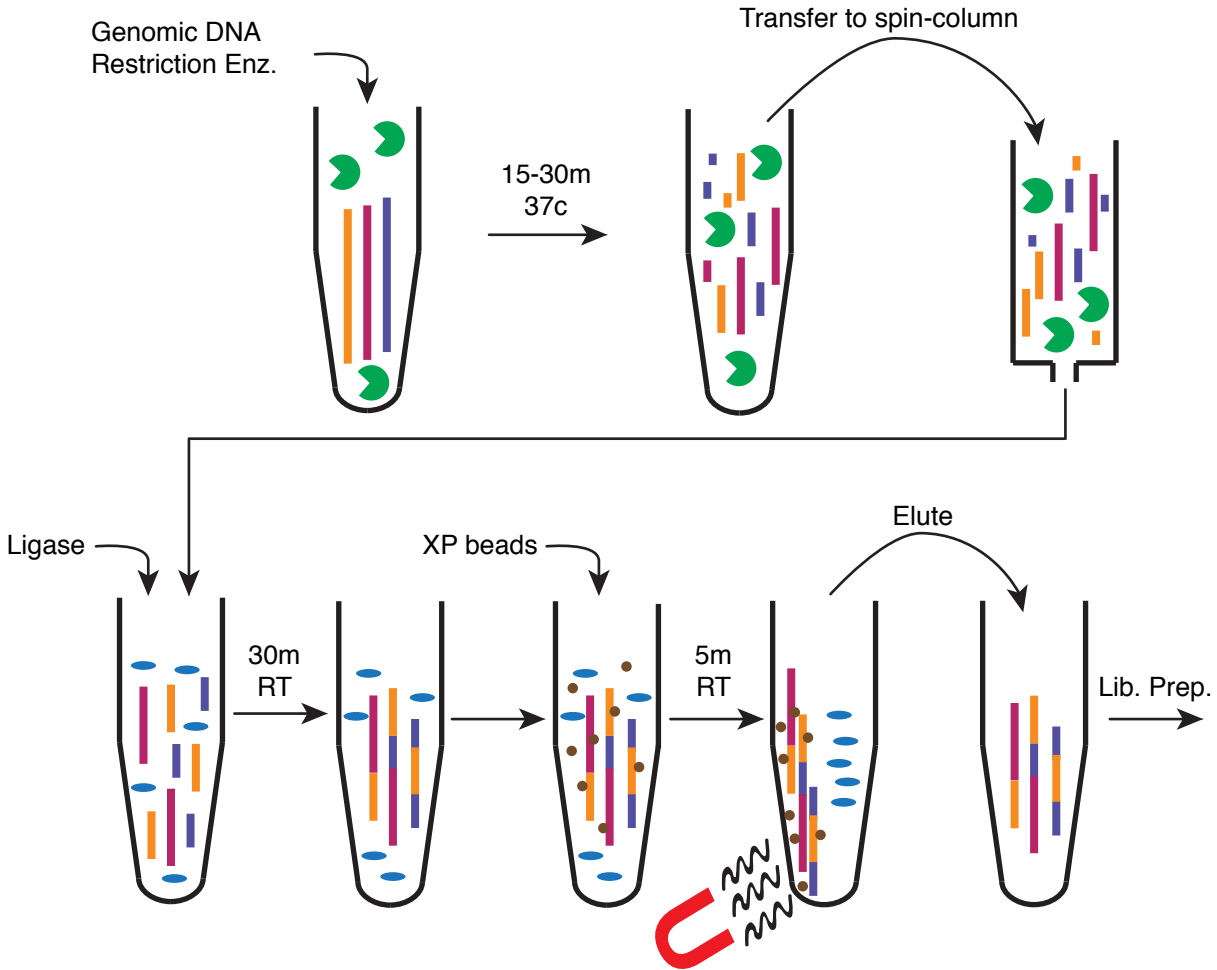


Figure 3.2: Schematic of SMURF-seq protocol. SMURF-seq consists of four steps: restriction enzyme digestion, spin-column clean-up, re-ligation of fragmented DNA, and Ampure XP beads clean-up.

restriction enzymes to fragment DNA molecules, over other fragmentation techniques, is that the fragmented molecules have a uniform ends (either overhangs with the same sequence or blunt-ends) and are thus compatible for ligation without an end-repair step in between.

2. Clean-up: the reaction containing the restriction enzymes and the fragmented DNA molecules is cleaned to wash out the enzymes and retain the DNA molecules. The choice of clean-up kit used, also determines the length of the DNA molecules that are retained. We used a spin-column based clean-up that typically retains molecules that are over  $\sim 70$  bp. However, other clean-up kits, such as bead-based kits, could also be used at this step.
3. Re-ligation: fragmented DNA molecules with uniform ends are ligated at random with T4 DNA ligase enzymes. The most important factor in a ligation reaction is the concentration of compatible DNA ends [1]. At high concentrations, the chances are higher for ligation between two molecules than a molecule self-ligating. At low concentrations, the chances are higher for self-ligation. Thus, the main consideration during the ligation step is the duration of the ligation reaction, as the molar concentration of DNA



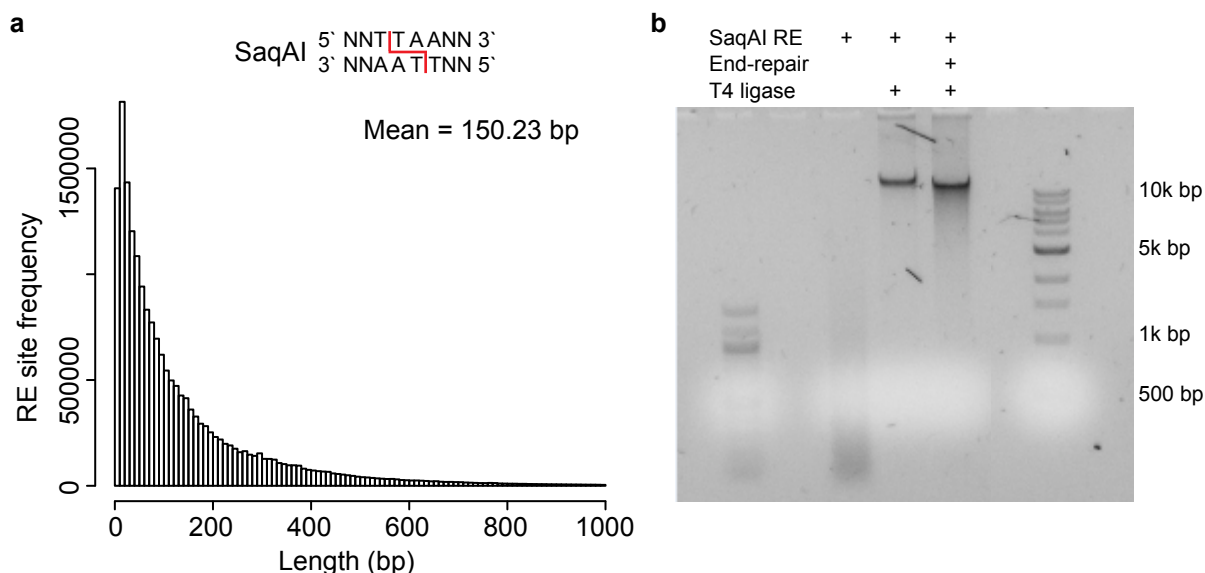


Figure 3.3: Restriction digestion and ligation of DNA molecules. (a) Distribution of length between restriction sites computed by measuring the distance between the recognition sites on the human reference genome. SaqAI recognizes the sequence TTAA and leaves a 2 bp overhang. (b) Negative gel image of fragmented and ligated normal diploid DNA using SaqAI restriction enzyme and T4 DNA ligase. Sticky-end and blunt-end ligation (by end-repair) of fragmented DNA are shown, and both yield ligated molecules of approximately the same length.

molecules decrease with time. Too little time would lead to insufficient ligation, resulting in molecules of length that do not achieve optimal SMURF-seq efficiency. On the other extreme, too much time would result in circular molecules that are incompatible with the most downstream library preparation process. A typical ligation reaction would contain both short and circularized molecules, and achieving a balance between these determines the efficiency of SMURF-seq. Other factors such as the temperature and buffer contents also affect the ligation process. In our experiments, the ligation reaction was performed at a DNA concentration of 25 ng/ $\mu$ l (500 ng of DNA in 10  $\mu$ l nuclease free water and 10  $\mu$ l DNA ligase) for 30 min.

4. Bead-based clean-up: the reaction containing the ligase enzymes and ligated DNA molecules is cleaned to retain only the ligated molecules. We used a bead-based clean-up at this step to avoid damage to long DNA molecules that are typical of spin-column based methods.

DNA molecules processed with the SMURF-seq protocol are compatible with any standard long-read library preparations kits that are available.

We also tested dsDNA Fragmentase enzymes (New England Biolabs) and acoustic shearing (Covaris) to fragment DNA. However, these methods require an additional end-repair step after fragmentation and the ligated molecules failed to reach the lengths we obtained by using restriction fragmentation (data not shown).

In our applications, we used SaqAI restriction enzyme, which recognizes the sequence TTAA and produces molecules with mean lengths of 150.2 bp (Fig. 3.3a). The fragmented DNA molecules are then ligated randomly to form longer molecules using T4 DNA ligase enzyme (Fig. 3.3b). In our experiments, the resulting long DNA molecules were sequenced using the Oxford Nanopore Technologies 1D DNA by ligation kit

(SQK-LSK108) or the rapid sequencing kit (SQK-RAD003) following the standard manufacturers protocol.

### 3.3 Mapping SMURF-seq reads

The reads sequenced using SMURF-seq can be mapped to a reference genome by first identifying short matches within the reads, corresponding to parts of the individual fragments, and then extending those to locate fragment boundaries. This is handled nicely using the seed-and-extend paradigm implemented in many existing long-read mapping tools.

#### 3.3.1 Simulating SMURF-seq reads to evaluate mapping programs

To test these mapping tools, we chose to create simulated reads with the technical characteristics we expect in idealized SMURF-seq data. We first selected a fragment length  $\ell$  and a number  $k$  of fragments per read. Then, for a given WGS nanopore data set, we took the set of mapped long reads as determined by BWA-MEM (with `-x ont2d` option). Each of the mapped reads was split into fragments of length  $\ell$  (with a random offset of 0 to  $\ell - 1$  at the start of the long read). Each fragment was validated by requiring that it did not overlap a deadzone in the genome (as determined by the deadzone program available from <https://github.com/smithlabcode/utis> for 40 bp). The reason for excluding deadzones is that even when a short fragment has a “known” mapping location when it is part of a longer read, we cannot compare its reported mapping location as a short fragment with that known location, since we expect any good mapping algorithm to identify that the fragment maps ambiguously. Among these validated fragments, subsets of  $k$  were sampled uniformly at random and concatenated (in random order and orientation) to form simulated SMURF-seq reads.

The first and last fragments in a read should be slightly easier to identify and map than the rest, since one of their boundaries is known. Using the above procedure, we select  $k = 20$  so that the simulated reads have a sufficient number of fragments to eliminate the influence of the first and last fragments in each read on the results. There is no need to have large  $k$  otherwise.

By lowering  $\ell$  and making the fragments shorter, the task of mapping the fragments becomes more challenging. Real SMURF-seq reads have fragment lengths determined by restriction site density, size selection and other aspects of the experiments. But in testing mapping algorithms and optimizing parameters, there is no disadvantage to making the task more challenging. We only need to be able to distinguish the relative performance of different mapping tools and parameter combinations. Real SMURF-seq reads have varying fragment lengths, but in evaluating mapping tools, there is no need to randomize fragment lengths. None of the algorithms we evaluated are capable of either deducing or leveraging the fact that all simulated fragments have the same length. We selected  $\ell = 100$ , which begins to challenge the various mapping strategies. These values of  $\ell$  are slightly lower than the average in real SMURF-seq data.

#### 3.3.2 Evaluating performance using simulated SMURF-seq reads

Within the simulated reads, the boundaries of each fragment are known *a priori*, as are their mapping locations. We used this information to evaluate mapping tools in terms of (1) how well they identify fragments purely for the purpose of counting molecules, which is the primary information used in CNV analysis, and (2) how well they identify individual mapping bases within reads. The latter criteria becomes important in challenging cases and will be increasingly important as fragment sizes are reduced.

Performance on identifying fragments: After mapping these simulated reads, each mapping result is called a predicted fragment. Each predicted fragment is considered a positive prediction, and we assume an arbitrary order over positive predictions. A positive prediction is a true positive if:

- The predicted fragment maps uniquely.
- The mapping locations of at least half the bases in the predicted fragment are equal to the original mapping locations for those bases, and those bases are all part of the same original fragment (we assume that it is unlikely for two fragments on a simulated read to have the same mapping location but opposite orientation, and thus do not check for the orientation of a fragment). In this case, we say the predicted fragment is associated with that original fragment.
- The predicted fragment is the first among predicted fragments associated the same original fragment.

False positives are predicted fragments that are not true positives. Any original fragment with no associated predicted fragment is a false negative. These criteria penalize splitting one original fragment or merging two original fragments. By defining true positives, false positives and false negatives we are able to calculate precision, recall, and F-score for a particular mapping strategy.

Performance on identifying individual mapping bases: After mapping simulated reads, each mapping result is decomposed into individual nucleotides and associated with a location in the genome. Those locations are retained. We keep multiplicities, so when two mapped fragments overlap in the genome we count certain nucleotides twice. These are the predicted positive bases in the reference. The condition positive bases are those known *a priori* from the simulation. The original fragment mapping locations may overlap in the reference genome, leading to multiplicities in the condition positive bases, but with low probability. The true positives are the intersection of the condition positive and the predicted positive bases. When there are multiplicities of mapped fragments and simulated fragments overlapping the same bases in the reference genome, this is determined by taking the smaller of the two values. After removing the true positives bases, the remaining predicted positive bases are false positives, and the remaining condition positive bases are false negatives. These criteria penalize mapping approaches that do not cover the entire simulated SMURF-seq reads, and also penalize approaches that predict fragments that overlap within the read. The true positives, false positives, and false negatives here allow us to assign precision and recall in terms of individual bases and corresponding F-scores. Although the reference bases for both predicted positive and condition positive could involve multisets, since our simulations used relatively low coverage this almost never happened.

### 3.3.3 Data sets for generating simulated SMURF-seq reads

To generate simulated reads we used the standard long reads from four sequencing runs (Flowcell ID: FAB42704, FAB42810, FAB49914, and FAF01253) in the public dataset available at <https://github.com/nanopore-wgs-consortium/NA12878/blob/master/Genome.md> [3, 7]. We downloaded the raw data from EBI (Run accession: ERR2184696, ERR2184704, ERR2184712, and ERR2184722) and base-called these with Guppy (version: 2.3.5).

### 3.3.4 Initial selection of mapping tools

We tested the following mapping tools: BWA-MEM[8], Minimap2[9], LAST[10], GraphMap[11], BLASR[12], rHAT[13], and LAMSA[14]. These were selected either because they are known to perform well on certain mapping tasks or have unique properties that plausibly could help in mapping SMURF-seq reads. We tested each of these using default parameters on simulated reads (see above) and downsampled real SMURF-seq reads (data not shown). Among these BWA-MEM, Minimap2, and LAST had higher accuracy on simulated

data, and the other tools identified at most 15 fragments per read on real data. Thus, we explored performance of BWA-MEM (0.7.17), LAST (963), and Minimap2 (2.15) in more detail, varying parameters to improve performance.

We remark that none of these tools were designed to map SMURF-seq reads; results we report here do not reflect the overall performance of the various mapping tools, only that the three aforementioned tools happened to perform relatively well on a task for which they were not directly designed for.

### 3.3.5 Detailed evaluation and parameter optimization

The selected mapping tools have variations on the following basic steps:

- Identifying seeds: All tools have a step of identifying seeds, which are short exactly matching parts of the reads. Choices in how seeds are defined and used are often made for mapping speed. The total size of SMURF-seq data sets is currently (relatively) small, so speed is not our primary concern. We favor the most sensitive seed strategy, but depending on implementation too many seed hits could lead to ambiguity later in the mapping process.
- Chaining seeds: The identified seeds are further extended and filtered to avoid aligning potentially false positive seed hits.
- Aligning within the chains: In this stage a Smith-Waterman alignment is performed, typically allowing users to specify a mismatch penalty along with penalties for both gap-open and gap-extend.
- Selecting best alignments: When high-scoring alignments overlap within a read, one of them (or both) could be trimmed or one is selected and the other discarded. The choices made here could lead to discarding entire fragments.

These mapping tools have several parameter options, in general, these are related to: (1) the seeding and chaining algorithm used by the individual tool. (2) The Smith-Waterman alignment scores, i.e. the match score, and the mismatch and indel penalty. The seeding and chaining parameters control the number of proto alignments that are further refined by aligning parts of the read to the reference genome using the specified alignment scores.

The Smith-Waterman alignment score used to align fragments to the reference genome is crucial for determining the optimal fragment length. On one extreme, a match score of 1 with a mismatch and indel penalty of 0 will result in one identified fragment covering the entire read and mapping perfectly, but will always map ambiguously. On the other extreme, a match score of 1 with a mismatch and indel penalty of  $-\infty$  will result in any mismatch or indel on the read to be considered as a fragment boundary. Therefore to align SMURF-seq reads, we need to determine optimal alignment scores to use.

In order to determine the optimal alignment score, we kept the seeding related parameters constant, and varied the alignment score combinations to perform a grid search. We varied the mismatch penalty from 1 to 6, gap open penalty from 0 to 4, and gap extend penalty from 1 to 4. The match score was fixed at 1. Thus for each tool we tested 120 ( $6 \times 5 \times 4$ ) combinations of alignment scores.

The seeding and chaining related parameters for each tool was set at follows (along with the four alignment scores):

- BWA-MEM: `-x ont2d -k 12 -W 12 -T 30`
- Minimap2: `-w 1 -m 10 -s 30`
- LAST (NEAR): `lastal -Q0 -e 20` and `last-split -m 1 -s 30`

We set the seeding and chaining parameters in a liberal manner to allow for higher sensitivity than the default parameter of each tool, and the minimum alignment score to output was set at 30.

After aligning the simulated reads, we calculated the average precision and recall, each for the mapped fragment locations and nucleotides, for the four datasets. The F-score was computed for each, and the mean

of the F-scores was used to determine the optimal alignment parameter for each tool. Based on these results BWA-MEM outperformed other tools for aligning SMURF-seq reads. BWA-MEM performed best with a mismatch, open, and extension penalty of 2, 1, 1 respectively.

To further refine the optimal alignment parameter for BWA-MEM, we aligned the simulated reads with parameter values around the value described above with a higher resolution. We varied the mismatch penalty from 1.5 to 2.5, and open and extend penalties from 0.5 to 1.5 in increments of 0.25. However, BWA-MEM does not accept floating point values for alignment score parameters. To overcome this, we scaled the alignment score proportionately to have integer values, i.e we varied the mismatch penalty from 6 to 10, open and extend penalties from 2 to 6, and fixed the match score at 4 (125 combinations). Based on these results, the highest accuracy was obtained with the mismatch, open, and extension penalty of 2.5, 1.5, 0.75 respectively (corresponding scaled values are 10, 6 and 3). We used these optimal alignment scores for mapping real SMURF-seq read, and all the CNV profiles presented are based on these.

## 3.4 Efficient CNV profiling using SMURF-seq

To demonstrate the utility of SMURF-seq, we generated CNV profiles of normal diploid and highly rearranged cancer genomes. The mapped fragments were grouped into variable length “bins” across the genome and bin counts were used to generate CNV profiles as described in [15, 16].

### 3.4.1 Normalizing restriction site bias

### 3.4.2 Accurate CNV profiles using SMURF-seq

We sequenced a normal diploid female genome with SMURF-seq, resulting in 270.8k reads (mean read length of 6.75 kb) in a single run. These reads were split into 7.28 million fragments (26.87 mean fragments per read). A CNV profile for this normal diploid genome, with the expected (approximately flat) appearance can be seen in Fig. 3.4a. We verified that the SMURF-seq procedure behaves similarly using the Rapid Sequencing Kit (the 213.38k sequenced reads had a mean read length of 3.9 kb, and were split into 2.81 million fragments). Next we applied SMURF-seq to the breast cancer line SK-BR-3, generating 147.0k reads with mean length of 7.62 kb, which were split into 4.52 million fragments (30.78 mean fragments per read). We then obtained a CNV profile using 5,000 bins, corresponding to an average bin size of approximately 600 kb (Fig. 3.4b).

To provide a quantification of accuracy in terms of individual CNV events we conducted whole-genome sequencing (WGS) on the same SK-BR-3 using Illumina (5.56 million reads; 130 bp, single-end). We used this to define a ground truth by calling CNV events for each of the pre-defined bins (both amplifications and deletions) based on segmented signal with a cutoff of 1.25/0.8 (Fig. 3.4b) [17, 18]. This resulted in 1,466 events (886 amplifications, 580 deletions) from 4,953 bins. We then called events using the identical procedure with SMURF-seq data from the same SK-BR-3 sample. The precision and recall for SMURF-seq relative to the Illumina calls was 0.982 and 0.988, respectively (Fig. 3.4c). Fig. 3.4d shows a zoom-in of a region with extreme copy number alterations. The bin ratios for the Illumina WGS and the SMURF-seq profiles are highly correlated (Pearson  $r = 0.99$ ; Fig. 3.4e). Replicates for these genomes show a high degree of reproducibility for these profiles (data not shown).

### 3.4.3 Concordant profiles from fewer countable fragments

Several cancer-related studies have employed CNV profiling based on low-coverage WGS [19, 20]. It has previously been demonstrated that 250k reads are sufficient for accurate genome-wide CNV profiling of single cells [21]. At the same time, the CNV profiles from a population of cells has been shown to have a high correlation with single-cell profiles [22, 21]. We reasoned that using 250k fragments for CNV profiling using a population of cells would give useful profiles if they remained sufficiently accurate. By down-sampling our SMURF-seq data, we verified that 10k reads, approximately 250k fragments, result in highly-correlated CNV profiles (Pearson  $r = 0.98$ ; Fig. 3.5a, b).

Given the total capacity of the MinION instrument, this indicates that multiple samples can effectively be barcoded and multiplexed in a single sequencing run. To verify this we sequenced two DNA samples (normal diploid female and SK-BR-3) in a single run. These samples were processed with SMURF-seq protocol and then barcoded following the standard library construction. After demultiplexing and mapping

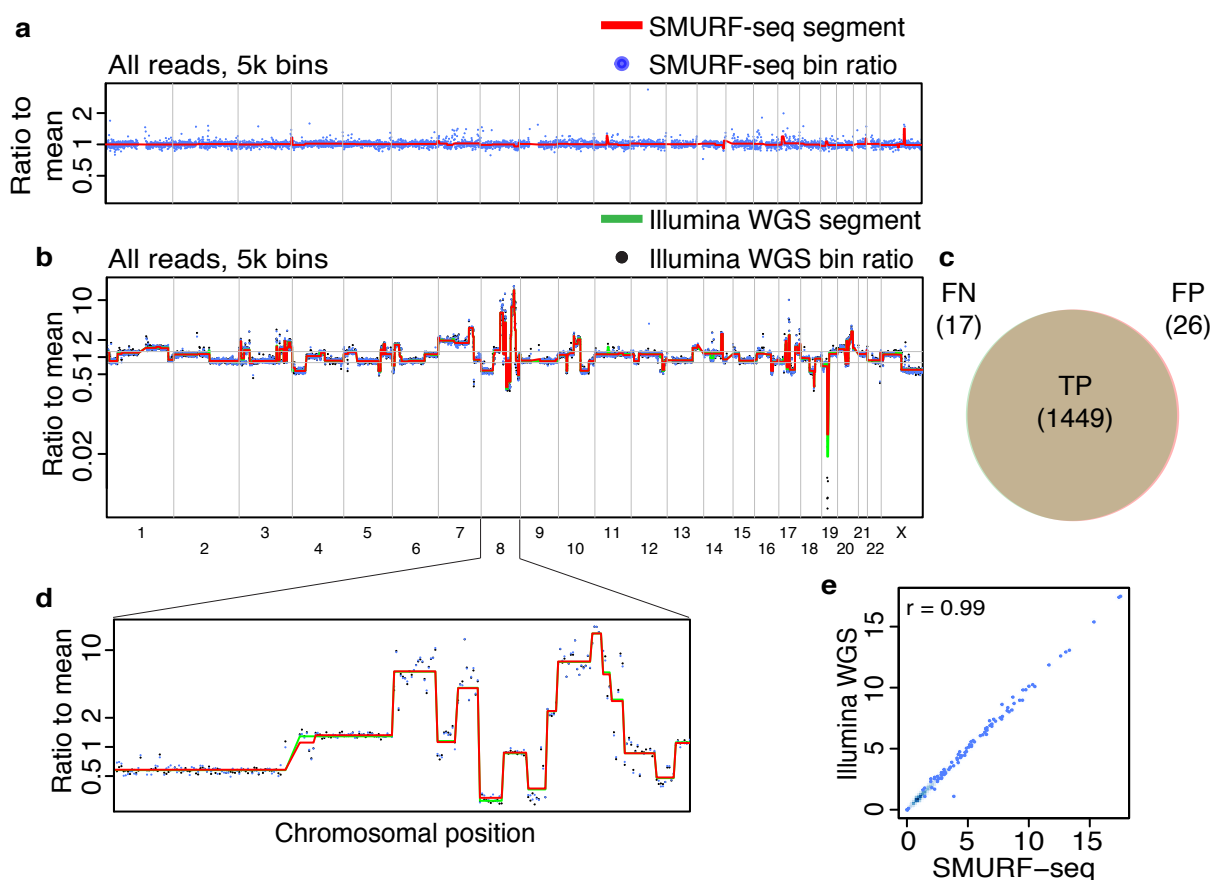


Figure 3.4: Accurate copy number profiles with SMURF-seq. (a) CNV profile of a normal diploid genome. Each blue point is a bin ratio to mean and the red line is the segmented bin ratio. (b) Superimposed CNV profiles of SK-BR-3 genome generated using SMURF-seq and Illumina WGS reads. (c) Venn diagram illustrating the accuracy of event calls using SMURF-seq compared with Illumina WGS. (d) Zoom-in of copy number changes on chromosome 8. (e) Scatter plot of bin ratio of SK-BR-3 genome using SMURF-seq and Illumina WGS reads. Pearson correlation of the data is shown.

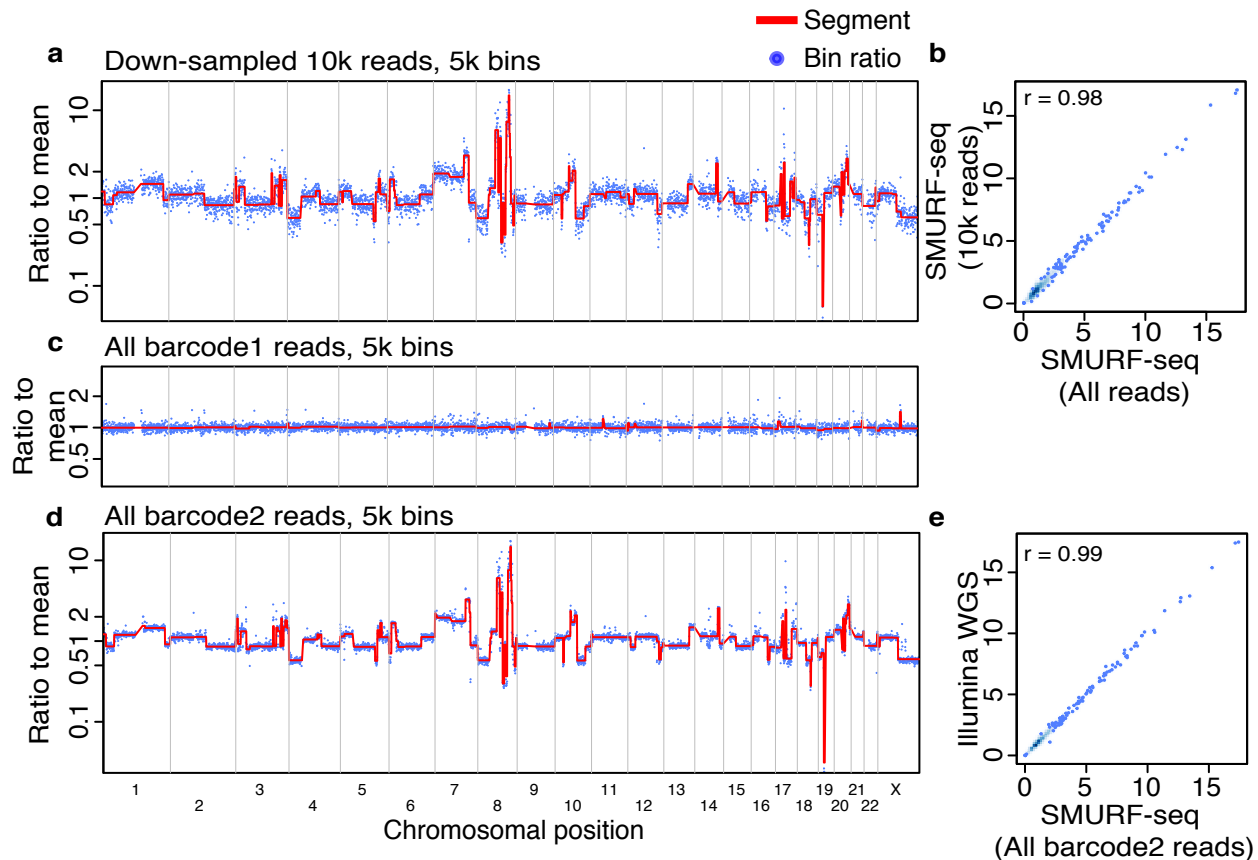


Figure 3.5: Multiple SMURF-seq CNV profiles by multiplexing in a single run. (a) CNV profile of SK-BR-3 genome with down-sampled 10k SMURF-seq reads. (b) Scatter plot of normalized bin counts of the original SMURF-seq data and data down-sampled to 10k SMURF-seq reads. Pearson correlation of the data is shown. (c) CNV profile of barcode01 (Normal diploid genome) reads. (d) CNV profile of barcode02 (SK-BR-3 cancer genome) reads. (e) Scatter plot of bin ratios of SK-BR-3 genome using multiplexed SMURF-seq and Illumina WGS reads.

the reads, the diploid genome had a CNV profile as expected (Fig. 3.5c) and the SK-BR-3 CNV profile was nearly identical to the profile obtained using Illumina WGS (Pearson  $r = 0.99$ ; Fig. 3.5d, e).

# Bibliography

- [1] Achilles Dugaiczyk, Herbert W Boyer, and Howard M Goodman. Ligation of ecori endonuclease-generated dna fragments into linear and circular structures. *Journal of molecular biology*, 96(1):171–184, 1975.
- [2] Philipp Euskirchen, Franck Bielle, Karim Labreche, Wigard P Kloosterman, Shai Rosenberg, Mailys Daniau, Charlotte Schmitt, Julien Masliah-Planchon, Franck Bourdeaut, Caroline Dehais, et al. Same-day genomic and epigenomic diagnosis of brain tumors using real-time nanopore sequencing. *Acta Neuropathologica*, 134(5):691–703, 2017.
- [3] Miten Jain, Sergey Koren, Karen H Miga, Josh Quick, Arthur C Rand, Thomas A Sasani, John R Tyson, Andrew D Beggs, Alexander T Dilthey, Ian T Fiddes, et al. Nanopore sequencing and assembly of a human genome with ultra-long reads. *Nature Biotechnology*, 2018.
- [4] John R Tyson, Nigel J O’Neil, Miten Jain, Hugh E Olsen, Philip Hieter, and Terrance P Snutch. Minion-based long-read sequencing and assembly extends the *caenorhabditis elegans* reference genome. *Genome Research*, 28(2):266–274, 2018.
- [5] M Muthukumar. Theory of capture rate in polymer translocation. *The Journal of Chemical Physics*, 132(19):05B605, 2010.
- [6] Meni Wanunu, Jason Sutin, Ben McNally, Andrew Chow, and Amit Meller. DNA translocation governed by interactions with solid-state nanopores. *Biophysical Journal*, 95(10):4716–4725, 2008.
- [7] Miten Jain, Sergey Koren, Karen H Miga, Josh Quick, Arthur C Rand, Thomas A Sasani, John R Tyson, Andrew D Beggs, Alexander T Dilthey, Ian T Fiddes, et al. Nanopore sequencing and assembly of a human genome with ultra-long reads, 2018.
- [8] Heng Li. Aligning sequence reads, clone sequences and assembly contigs with bwa-mem. *arXiv preprint arXiv:1303.3997*, 2013.
- [9] Heng Li. Minimap2: pairwise alignment for nucleotide sequences. *Bioinformatics*, 34(18):3094–3100, 2018.
- [10] Szymon M Kiełbasa, Raymond Wan, Kengo Sato, Paul Horton, and Martin C Frith. Adaptive seeds tame genomic sequence comparison. *Genome research*, 21(3):487–493, 2011.
- [11] Ivan Sović, Mile Šikić, Andreas Wilm, Shannon Nicole Fenlon, Swaine Chen, and Niranjana Nagarajan. Fast and sensitive mapping of nanopore sequencing reads with GraphMap. *Nature Communications*, 7:11307, 2016.



- [12] Mark J Chaisson and Glenn Tesler. Mapping single molecule sequencing reads using basic local alignment with successive refinement (blasr): application and theory. *BMC bioinformatics*, 13(1):238, 2012.
- [13] Bo Liu, Dengfeng Guan, Mingxiang Teng, and Yadong Wang. rHAT: fast alignment of noisy long reads with regional hashing. *Bioinformatics*, 32(11):1625–1631, 2015.
- [14] Bo Liu, Yan Gao, and Yadong Wang. LAMSA: fast split read alignment with long approximate matches. *Bioinformatics*, 33(2):192–201, 2017.
- [15] Timour Baslan, Jude Kendall, Linda Rodgers, Hilary Cox, Mike Riggs, Asya Stepansky, Jennifer Troge, Kandasamy Ravi, Diane Esposito, B Lakshmi, et al. Genome-wide copy number analysis of single cells. *Nature Protocols*, 7(6):1024, 2012.
- [16] Jude Kendall and Alexander Krasnitz. *Computational Methods for DNA Copy-Number Analysis of Tumors*, pages 243–259. Springer New York, New York, NY, 2014.
- [17] Angel E Dago, Asya Stepansky, Anders Carlsson, Madelyn Luttgen, Jude Kendall, Timour Baslan, Anand Kolatkar, Michael Wigler, Kelly Bethel, Mitchell E Gross, et al. Rapid phenotypic and genomic change in response to therapeutic pressure in prostate cancer inferred by high content analysis of single circulating tumor cells. *PloS ONE*, 9(8):e101777, 2014.
- [18] Jesse L Berry, Liya Xu, A Linn Murphree, Subramanian Krishnan, Kevin Stachelek, Emily Zolfaghari, Kathleen McGovern, Thomas C Lee, Anders Carlsson, Peter Kuhn, et al. Potential of aqueous humor as a surrogate tumor biopsy for retinoblastoma. *JAMA ophthalmology*, 135(11):1221–1230, 2017.
- [19] Geoff Macintyre, Teodora E Goranova, Dilrini De Silva, Darren Ennis, Anna M Piskorz, Matthew Eldridge, Daoud Sie, Liz-Anne Lewsley, Aishah Hanif, Cheryl Wilson, et al. Copy number signatures and mutational processes in ovarian carcinoma. *Nature Genetics*, 50(9):1262, 2018.
- [20] Tanjina Kader, David L Goode, Stephen Q Wong, Jacquie Connaughton, Simone M Rowley, Lisa Devereux, David Byrne, Stephen B Fox, Gisela Mir Arnau, Richard W Tothill, et al. Copy number analysis by low coverage whole genome sequencing using ultra low-input DNA from formalin-fixed paraffin embedded tumor tissue. *Genome Medicine*, 8(1):121, 2016.
- [21] Timour Baslan, Jude Kendall, Brian Ward, Hilary Cox, Anthony Leotta, Linda Rodgers, Michael Riggs, Sean D’Italia, Guoli Sun, Mao Yong, et al. Optimizing sparse sequencing of single cells for highly multiplex copy number profiling. *Genome Research*, 25(5):714–724, 2015.
- [22] Nicholas Navin, Jude Kendall, Jennifer Troge, Peter Andrews, Linda Rodgers, Jeanne McIndoo, Kerry Cook, Asya Stepansky, Dan Levy, Diane Esposito, et al. Tumour evolution inferred by single-cell sequencing. *Nature*, 472(7341):90, 2011.